

Metabolomics approach for determining growth-specific metabolites based on Fourier transform ion cyclotron resonance mass spectrometry

Hiroki Takahashi · Kosuke Kai · Yoko Shinbo ·
Kenichi Tanaka · Daisaku Ohta · Taku Oshima ·
Md. Altaf-Ul-Amin · Ken Kurokawa ·
Naotake Ogasawara · Shigehiko Kanaya

Received: 12 February 2008 / Revised: 7 May 2008 / Accepted: 20 May 2008 / Published online: 16 June 2008
© The Author(s) 2008

Abstract Fourier transform ion cyclotron resonance mass spectrometry (FT-ICR/MS) is the best MS technology for obtaining exact mass measurements owing to its great resolution and accuracy, and several outstanding FT-ICR/MS-based metabolomics approaches have been reported. A reliable annotation scheme is needed to deal with direct-infusion FT-ICR/MS metabolic profiling. Correlation analyses can help us not only uncover relations between the ions but also annotate the ions originated from identical metabolites (metabolite derivative ions). In the present study, we propose a procedure for metabolite annotation on direct-infusion FT-ICR/MS by taking into consideration the classification of metabolite-derived ions using correlation analyses. Integrated analysis based on information of isotope relations, fragmentation patterns by MS/MS analysis, co-occurring metabolites, and database searches (KNApSACk and KEGG) can make it possible to annotate ions as metabolites and estimate cellular conditions based on metabolite composition.

A total of 220 detected ions were classified into 174 metabolite derivative groups and 72 ions were assigned to candidate metabolites in the present work. Finally, metabolic profiling has been able to distinguish between the growth stages with the aid of PCA. The constructed model using PLS regression for OD₆₀₀ values as a function of metabolic profiles is very useful for identifying to what degree the ions contribute to the growth stages. Ten phospholipids which largely influence the constructed model are highly abundant in the cells. Our analyses reveal that global modification of those phospholipids occurs as *E. coli* enters the stationary phase. Thus, the integrated approach involving correlation analyses, metabolic profiling, and database searching is efficient for high-throughput metabolomics.

Keywords Fourier transform ion cyclotron resonance mass spectrometry · Metabolomics · Metabolite annotation · Cellular conditions · Correlation network

Electronic supplementary material The online version of this article (doi:10.1007/s00216-008-2195-5) contains supplementary material, which is available to authorized users.

H. Takahashi · Y. Shinbo · K. Tanaka · T. Oshima ·
M. Altaf-Ul-Amin · K. Kurokawa · N. Ogasawara ·
S. Kanaya (✉)
Graduate School of Information Sciences,
Nara Institute of Science and Technology,
8916-5, Takayama,
Ikoma, Nara 630-0192, Japan
e-mail: skanaya@gtc.naist.jp

K. Kai · D. Ohta
Graduate School of Life and Environmental Sciences,
Osaka Prefecture University,
Sakai 599-8531, Japan

Introduction

Comprehensive metabolomics is clearly distinct from conventional metabolism studies in that it addresses whole cellular activities rather than just focusing on enzymes, reactions, or metabolites. Over the past decade methods that offer both high resolution and sensitivity for the measurement of a vast number of metabolites have been established and two major approaches, targeted and nontargeted metabolomics studies, have been developed in metabolome studies [1, 2]. Targeted metabolomics plays a crucial role in understanding the primary effects of genetics alternations based on restricted information of a class of metabolites,

and analytical procedures often need to include processes for identification and quantification of selected metabolites. Only recent advances in mass spectrometry have allowed nontargeted metabolomics, which is intended for unbiased analyses such as mapping metabolite profiles in the whole cellular processes in given organisms.

Fourier transform ion cyclotron resonance mass spectrometry (FT-ICR/MS) is the best MS technology for obtaining exact mass measurements owing to its great resolution and accuracy [3, 4], and several outstanding FT-ICR/MS-based metabolomics strategies have been reported [5–10]. Development of a general scheme for FT-ICR/MS-based metabolic profiling, with the aid of its potential for the high resolution measuring power together with ion signal intensity information, should thus make a significant contribution to metabolomics studies. To attain the purpose of and to understand the cell system based on the components of metabolites, we apply chemometrics and bioinformatics approaches to FT-ICR/MS data. Among a variety of metabolomics strategies, FT-ICR/MS offers a unique opportunity in nontargeted metabolomics studies owing to its extreme accuracy (below 1 ppm) in the mass measurement. Thus, chemical formulas and molecular identities of metabolites can be predicted with the aid of high precision mass spectrometry (MS) data and can also be easily linked to reported metabolites.

Metabolomics research currently confronts a problem associated with high-throughput data acquisition technologies including chromatography-coupled mass spectrometry (MS) and FT-ICR/MS which have facilitated simultaneous detection and quantification of a large number of metabolite-derived peaks without metabolite assignment [11]; a very similar situation has arisen in genomics research in that technologies for determination of the nucleotide sequence in the whole genome has progressed without annotations of gene functions [12]. Progress in annotation of metabolites in metabolomics can bridge the gap between the data and their biological interpretation. The problem with annotation of metabolites is that there is only a piece of information about peaks corresponding to precise molecular weight for metabolite-derived ions in MS, but when we measure quantities of ions in a time series experiment, metabolite-derived ions such as isotope ions and multivalent ions could be categorized by correlations between ions originated from identical metabolites, which can lead to more precise annotation of ions. Thus, correlation analysis of ions may be a powerful approach to annotation of metabolites in metabolomics.

In the present study, we propose a procedure for metabolite annotation using the data obtained from FT-ICR/MS by taking classification of metabolite-derived ions into consideration. Here, we perform the nontargeted comprehensive analysis of metabolomics for the time series

measurements in *Escherichia coli*, and discuss a metabolic profiling scheme on the basis of FT-ICR/MS analyses furnished with a bioinformatics scheme including data preprocessing, classification of ions originated from identical metabolites, and supervised and unsupervised learning algorithms for metabolomics.

Experimental

Strains and growth conditions

The strain used in this study was *E. coli* K-12 W3110. An aliquot (8 ml) of an overnight liquid culture of W3110 in LB medium at 37 °C was inoculated into in 2 l LB (pH 7.4) medium in a 3-l jar fermenter. Cells were grown continuously at 37 °C for ca. 12 h, adjusting the agitation speed to 300 rpm with fixed 2 l min⁻¹ air flow rate. Growth was monitored by measuring the optical density at 600 nm (OD₆₀₀).

Sample preparation

A culture medium was passed through a 0.45- μ m-pore-size filter (Durapore Membrane, Millipore). Residual *E. coli* cells on the filter were washed with Milli-Q water and then plunged into 2 ml methanol [13]. After sonication for 1 min, the methanol solution was kept at 4 °C for ca. 20 h. The solution was then filtered through disposable membrane filter units (DISMIC-13JP, ADVANTEC), evaporated, and stored at -80 °C until use. Upon FT-ICR/MS analysis, the extracts were dissolved in 50% (v/v) acetonitrile/water. A set of 2,4-dichlorophenoxy acetic acid ([M-H]⁻=218.96212), ampicillin ([M-H]⁻=348.10235), 3-[(3-cholamidopropyl)dimethylammonio]propanesulfonic acid ([M-H]⁻=613.38920), and tetra-*N*-acetylchitotetraose ([M-H]⁻=829.32078) were used as the internal mass calibrants (IMCs) in the negative ion mode analysis.

FT-ICR/MS conditions

Mass analysis was done in the negative ion mode using an IonSpec Explorer FT-ICR/MS (IonSpec) equipped with a 7-T actively shielded superconducting magnet. Ions were generated from an ESI source with a fused silica needle of 0.005-inch i.d. Samples were infused using a Harvard syringe pump model 22 at a flow rate of 0.5 to 1.0 μ l min⁻¹ through a 100- μ l Hamilton syringe. All the experimental events were controlled using Omega8 software (IonSpec). Briefly, the potentials on the electrospray emitters were set to -3.0 kV for the negative electrosprays. The base pressure in the source region was approximately 5 \times 10⁻⁵ torr (1 torr=133.3 Pa). For the negative electrosprays, sample solutions were prepared in 50% (v/v) acetonitrile/water with 0.1%

(v/v) of ammonium hydroxide. Ionized metabolites were accumulated for a period of 2,500–5,000 ms in a hexapole ion trap/guide and transferred through a radiofrequency-only quadrupole into the FT-ICR cell in the superconducting magnetic field, where they were again trapped. The direct current potentials in the negative ion mode analyses were 2 V during the ion accumulation and –2 V for the ion transfer into the FT-ICR cell. These ions trapped in the hexapole were extracted for transfer into the FT-ICR cell. In the negative ion modes, the potentials on the extraction plate were –12 V during the ion trapping and were reversed to 2 V for the extraction. The base pressure in the analyzer region was set to approximately 4×10^{-10} torr. ESI-MS spectra were acquired over the m/z range 55–1,000 from 1,024,000 independent data points. MS/MS analyses were done using the sustained off-resonance irradiation SORI-CID methods [14, 15]. SORI R_f was set at 0.5–1.5 V, and the N_2 collision gas was used with a 400-ms pulse.

FT-ICR/MS data processing and data analyses

The first requirement for the success of metabolomics is the ability to mine the generated data and to perform reliable and comparative analysis. To attain this, we have developed a bioinformatics scheme (DrDMASS+) consisting of four stages: (i) peak correction, (ii) multivariate data processing, (iii) unsupervised learning such as principal component analysis (PCA) and batch-learning SOM (BL-SOM), and (iv) supervised learning such as partial least squares (PLS) regression. DrDMASS+ and its instruction manual are freely available at <http://kanaya.naist.jp/DrDMASSplus/>.

- (i) Peak correction. Though FT-ICR/MS affords extremely high resolution m/z values, analytical data fluctuations are generally associated with the m/z values at the three or four decimal places level. So, initially, appropriate m/z values must be estimated from the observed m/z values. The experimental m/z values of the IMCs were fixed to their theoretical values, and the m/z error calibration data were reflected in the m/z compensation for all other ion species in each spectral scan.
- (ii) Multivariate data processing. After compensating m/z values, ion peak matching among ten independent scans was done for repeated identifiable m/z values. The threshold levels of ion appearance frequencies were freely adjustable. The intensity values of repeatedly observed ions were converted into percentage values of total ion intensity. Thus, metabolomics data from a single biological sample consisted of averaged m/z values with intensity information from ten spectral scans.
- (iii) Unsupervised learning. PCA is a multivariate method to project a distribution of data points in a multi-

dimensional space into a space of fewer dimensions and BL-SOM is a method to classify such data points into groups (grids) accommodating similar decrease/increase patterns [16, 17].

- (iv) Supervised learning. PLS is a method for linearly relating a data matrix \mathbf{X} ($M \times N$) to a vector \mathbf{y} ($M \times 1$) where M and N represent the number of samples and parameters, respectively. The PLS model is represented by Eqs. (1) and (2).

$$\mathbf{X} = \sum_{k=1}^L \mathbf{t}_k \mathbf{p}_k^T + \mathbf{E} \quad (1)$$

$$\mathbf{y} = \sum_{k=1}^L \mathbf{t}_k q_k + \mathbf{e} \quad (2)$$

Here, \mathbf{p}_k and q_k are called the loading vector of \mathbf{X} , and the coefficient of \mathbf{y} for the k th component, respectively. L is the number of components and \mathbf{t}_k is a score vector for the k th component. \mathbf{E} ($M \times N$) and \mathbf{e} ($M \times 1$) represent the residual matrix and vector, respectively. The number of PLS components, L , is determined to maximize a predicted correlation coefficient (R_{pred}) by leave-one-out cross-validation for each component according to Eq. (3):

$$R_{\text{pred}} = 1 - \frac{\sum (y_{\text{obs}} - y_{\text{pred}})^2}{\sum (y_{\text{obs}} - \bar{y}_{\text{obs}})^2} \quad (3)$$

Here, y_{obs} is an experimental y value, y_{pred} is a predicted y value, and \bar{y}_{obs} is the mean of y_{obs} . The PLS equations (Eqs. (1) and (2)) can also be transformed into a linear form represented by Eq. (4) [18]:

$$\mathbf{y} = \mathbf{X}\mathbf{b} + \mathbf{f} \quad (4)$$

Here, \mathbf{b} is a regression coefficient vector and its elements are represented by b_j ($j=1,2,\dots,N$).

DPCLUS

DPCLUS is a graph clustering software that can extract densely connected clusters using an algorithm that is based on density and periphery tracking of clusters [19]. It is also necessary to provide a value of minimum density we allow for the generated clusters (d), a minimum value for cluster property that determines the nature of periphery tracking (cp_{in}), and a minimum number of objects that we want in a cluster. DPCLUS is freely available at <http://kanaya.naist.jp/DPCLUS/>.

Species–metabolite relationship database

We have accumulated the information of 41,644 species–metabolite pairs encompassing 21,118 metabolites and 13,094 species in the KNApSack database (as of 1

February 2008) [20]. Information on metabolites in the database can be searched by metabolite name, organism, molecular weight, molecular formula, and mass spectral data taking the ionization modes ($[M+NH_4]^+$, $[M+Na]^+$, $[M+K]^+$, $[M+H]^+$, and $[M-H]^-$) into consideration. Furthermore, the KNApSAcK package installed in the user's computer provides tools for analyzing their own datasets of mass spectra provided the files that contain the data are prepared according to the program's instructions. This database system and its online manual are freely available at <http://kanaya.naist.jp/KNApSAcK/>.

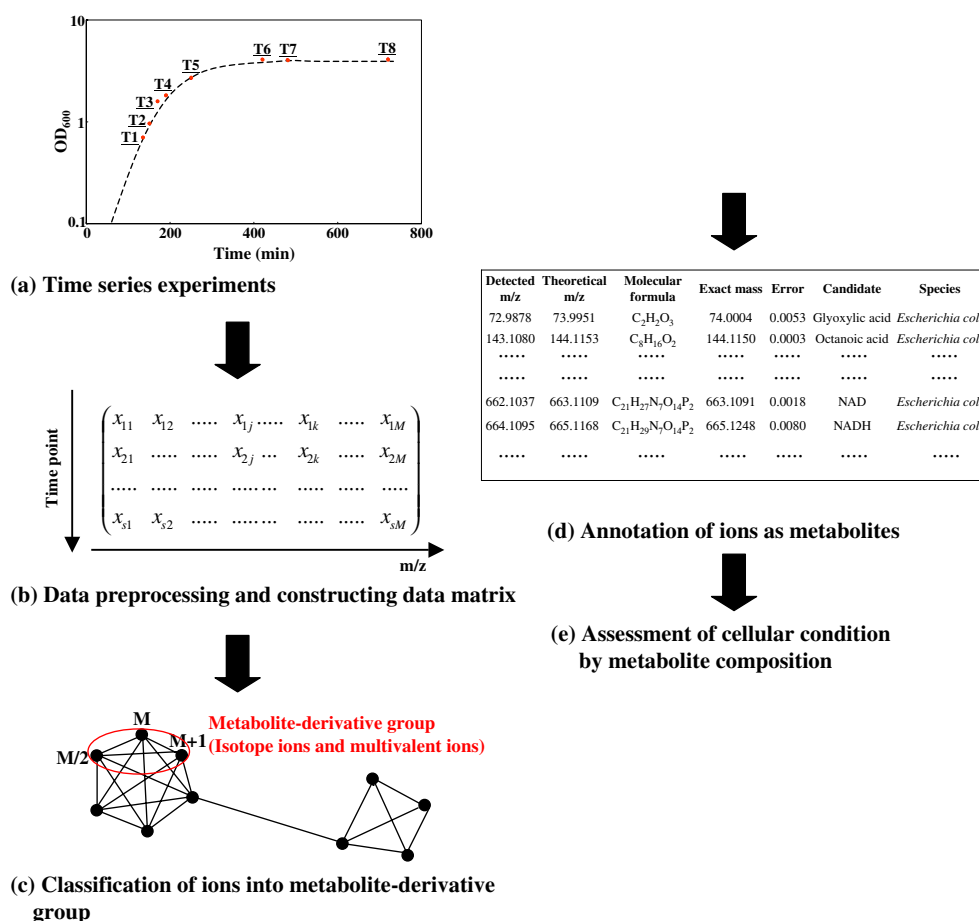
Results and discussion

Data processing of FT-ICR/MS: from data acquisition to assessment of cellular conditions according to metabolite composition

The concept of FT-ICR/MS data processing from data acquisition of a time series experiment to describe cellular conditions from exponential to stationary growth phase by metabolites consists of five steps (Fig. 1). Time series

experiments are a popular method for studying a wide range of biological systems. In bacteria, there are a few reported papers which comprehensively analyzed bacteria intrametabolites [21]. However, to our knowledge there are no papers about bacteria which address total intrametabolic profiling. In order to elucidate intrametabolite profiling in a whole cell, we performed the time series experiment in *E. coli* (Fig. 1a). Samples were collected at 135, 150, 170, 190, 250, 420, 480, and 720 min postinoculation (which correspond to T1, T2, T3, T4, T5, T6, T7, and T8, respectively), and metabolites were extracted, and measured by FT-ICR/MS. FT-ICR/MS raw data were processed for differential metabolomics according to the peak correction and peak matching of the DrDMASS+ program. We selected m/z values whose appearance frequencies were higher than 50% among ten scans. Thus, differential metabolomics was studied in terms of corrected m/z values with average signal intensities of reproducible ions from ten independent spectral data. The observed m/z values for ions individual measurements in the time series experiment were calibrated with those of internal standards [8]. Peak matchings were carried out to make a matrix consisting of intensities for m/z values and time points (Fig. 1b) utilizing

Fig. 1 Data processing scheme consisting of five steps. **a** Time series experiments in *E. coli*. The growth curve shows eight time points (135, 150, 170, 190, 250, 420, 480, and 720 min postinoculation corresponding to T1, T2, T3, T4, T5, T6, T7, and T8, respectively), at which samples were taken, and metabolites were extracted, and measured by FT-ICR/MS. **b** Data structure after data preprocessing by DrDMASS+ including peak correction and peak matching. M and s shows the number of detected ions and samples, respectively. **c** Classification of ions into metabolite derivative groups by DPCLUS based on the correlations between detected ions. **d** Annotation of ions by searching metabolite databases (KNApSAcK and KEGG). **e** Assessment of cellular conditions according to metabolite composition by using multivariate analyses



a metabolomics platform, based on FT-ICR/MS incorporating the metabolite profiling tool DrDMASS+. After the processing step, 220 independent ions were detected in the negative ion mode analysis. Thus, our time series data matrix consists of intensities of 220 independent ions corresponding to metabolites for eight measurement points.

There are many ions originated from identical metabolites, i.e., isotope ions and multivalent ions. If detected ions are classified into identical metabolite-derived ion groups, we can use further information for annotating chemical structures in metabolites because isotope pattern allows us to estimate the number of carbons in molecular formulas for metabolites, and the real number of metabolites included in samples can also be estimated. This step was carried out by DPClus software (Fig. 1c). After classification of ions into specific metabolite derivative groups, we performed annotation of ions as metabolites using public natural compound databases, KNApSack [20] and KEGG [22–24] (Fig. 1d), and cellular conditions were characterized by the composition of metabolites using two approaches, supervised and unsupervised learning. Cellular condition could be assessed by the metabolite composition using principal component analysis (PCA), and the relationship between cell densities and the metabolite composition, reflecting transition from exponential to stationary phases, could be understood by using partial least squares (PLS) regression (Fig. 1e). Marker metabolites significant in exponential and stationary growth were determined using PLS regression.

Classification of ions into metabolite derivative groups

The difference of m/z value between isotope ions originated from carbon atom (1.0033 u) is a clue for determining whether or not the ions are originated from identical metabolites. Furthermore, ions, originated from identical metabolites, occurring in different ion valence are also detected. Isotope intensity pattern of a metabolite in an MS chart can serve as a powerful additional constraint for removing wrong elemental composition candidates [25]. When intensities of ions are correlated to each other in a time series experiment, those ions would be expected to be originated from an identical metabolite. Tautenhahn et al. [26] successfully combined highly correlated pairs of mass signals in LC-MS to chemical relation hypothesis groups. Thus, taking into consideration the differences of m/z values for ions and correlation of time series profiles of ions, isotope ions can be classified into metabolite derivative groups, which lead to estimation of molecular formula of metabolites. To attain this, we visualized all correlations in a time series experiment between ions. Pairwise ion–ion correlations were calculated by Pearson's correlation coefficient (r) [27]. We extracted a set of 742 unique binary relations involving 148 ions by the threshold

$r \geq 0.9$ ($p < 2.3 \times 10^{-3}$, $n=8$) and visualized this by using the graph-clustering method called DPClus. Out of total 220 detected ions, 72 ions do not show significant correlation with other ions. Figure 2 shows the configuration of the 742 relations including 148 ions assigned to 11 isolated clusters (ID=1 to 11). Two largest isolated subgraphs consisting of 43 and 28 ions, respectively, can be characterized by six clusters (ID=1–1 to 1–6) and three clusters (ID=2–1 to 2–3), of size > 2 , which are all complete graphs where an edge connects every pair of distinct vertices within the same cluster. Ions assigned to multiple complete subgraphs are depicted by blue nodes. Relations between ions and cluster IDs are listed in the Electronic supplementary material (Table S1).

We assume that ions which belong to the same cluster and have appropriate m/z difference of ^{13}C and certain valences could be considered to have originated from identical metabolites. Initially, to determine isotopic ion pairs, we searched ion pairs under conditions that the ion pairs have not only correlation with each other but also appropriate m/z difference for certain k -valence, i.e., $\text{M}^- + \text{H}^+ = 2\text{M}^{2-} + 2\text{H}^+ = \dots = k\text{M}^{k-} + k\text{H}^+$. Furthermore, to determine ion pairs originated from identical metabolites, our search was extended to ions other than isotope ions. Thus, 19 metabolite derivative groups consisting of multiple ions including isotope and multivalent ions were identified (Fig. 2, surrounded by red broken lines). In total, 148 ions were classified into 102 metabolite derivative groups which include isotope ions and multivalent ions.

Annotation of ions

The concept of metabolite annotation comprises mass spectral annotation and biological metadata annotation including description of actual experimental conditions that help unravel the biological role of metabolites by their changes in levels in response to genetic and environmental perturbation [28, 29]. In the present study, we use the term 'metabolite annotation' to describe a procedure of providing chemical characterization to individual metabolite-derived ions; thus our annotation procedure can be classified as a mass spectral annotation, which is important for interpretation of cellular conditions according to metabolite compositions. There are two distinct ways to provide metabolite annotation: an exhaustive computation of all chemically possible isomeric structures or a query of databases for known natural compounds. In the present study, we annotated ions based on the latter method using additional evidence of chemical information such as MS/MS fragmentations. Three publicly available databases concerning natural products are PubChem [30], KEGG, and KNApSack. The PubChem database is comprised of records for over 19.6 million compounds with over 11 million unique structures including small molecules, par-

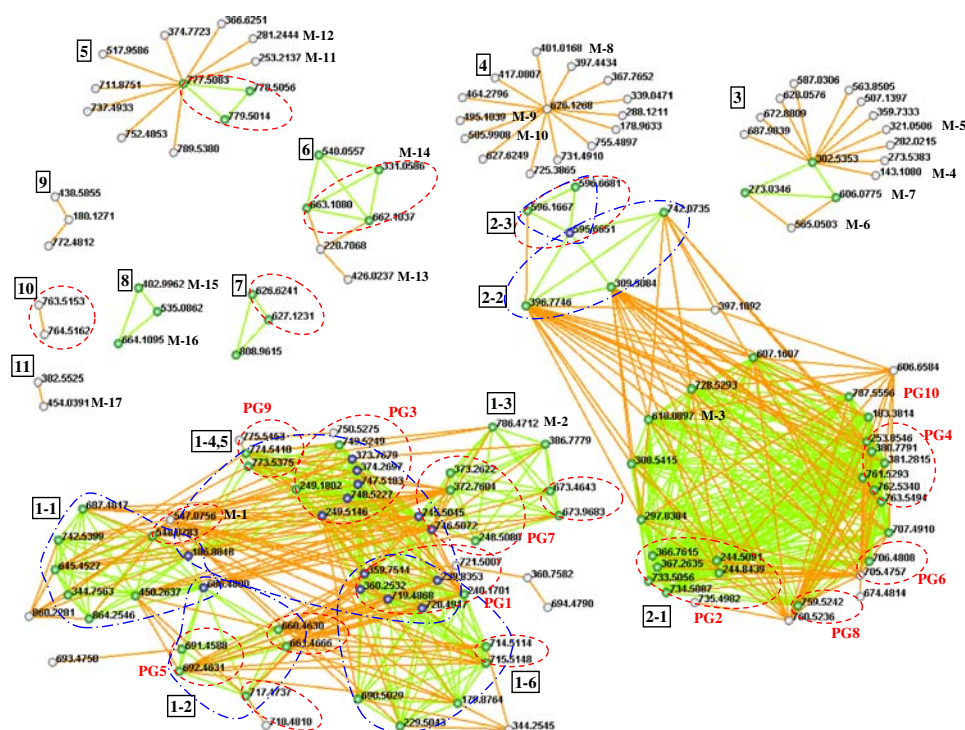


Fig. 2 Correlation analyses based on the graph clustering. A graph sharing correlation between ions and densely connected clusters. Each boxed black number (1–11) corresponds to a cluster ID detected by the graph clustering. Each node corresponds to an ion with m/z value indicated. The colors of nodes represent the ions within a cluster (green), the common ions among clusters (blue), and the other ions (silver). The intracluster edges are green and intercluster on the other edges are orange. The thick blue broken circles show the clusters 1–1, 1–2, 1–3, 1–4, 5, 1–6, 2–1, 2–2, and 2–3. The red dotted circles show isotope ions. PG1–PG10 are shown in red. M-1 to M-17 near the nodes

are the identities of ions which have candidates according to the KNApSack search: M-1, dTDP-L-rhamnose; M-2, BE 32030B; M-3, ADP-L-glycero-beta-D-manno-heptopyranose; M-4, octanoic acid; M-5, dTMP; M-6, UDP-D-glucose, UDP-D-galactose; M-7, UDP-N-acetyl-D-mannosamine, UDP-N-acetyl-D-glucosamine; M-8, dTDP; M-9, kinamycin A, kinamycin C; M-10, ATP, dGTP; M-11, omega-cycloheptanenoic acid; M-12, oleic acid, *cis*-11-octadecanoic acid, omega-cycloheptylundecanoic acid; M-13, adenosine 3',5'-bisphosphate, ADP, dGDP; M-14, NAD; M-15, UDP; M-16, NADH; M-17, antibiotic MI 178–34F18A2, antibiotic MI 178–34F18C2

ticularly diagnostic and therapeutic agents. In our study, ions are natural compounds and it is better to search the databases that contain natural products. In KEGG, the metabolic pathways are constructed by interspecies gene relations such as orthologs and paralogs, so metabolite–species relations can be obtained via information of enzymes. The KEGG database focuses on metabolites related to known metabolic pathways and includes around 13,000 metabolites. On the other hand, the relationships between metabolites and their biological origins have been addressed systematically in the KNApSack database, which has accumulated 41,644 records (species–metabolite pairs) encompassing 21,118 metabolites and 13,094 species (as of 1 February 2008). The total number of secondary metabolites for which molecular structures have been elucidated is estimated to be 50,000 [31]. So, around 42% of metabolites have been compiled in the database and this is considered to be enough for searching candidates including species information. As the first stage, we searched metabolites in two databases (KEGG and KNApSack) by molecular weights estimated from m/z values for ions.

Isotope patterns allow us to estimate the number of carbons in molecular formulas for metabolites because natural compounds on earth reflect the natural abundance of stable elemental isotopes, such as ^{13}C (which is found at approximately 1.07% of the most frequent isotope ^{12}C) [32]. The abundance of isotope ions is dependent on the actual elemental composition and can therefore serve as a powerful filter in calculating unique elemental compositions from mass spectral data [33]. In view of rigorous atomic mass, mass differences between isotopes of atoms are not identical, e.g., mass differences between ^1H and ^2H , ^{12}C and ^{13}C , and ^{14}N and ^{15}N are 1.0063 u, 1.0033 u, and 0.9970 u, respectively. Several software methods calculate isotope patterns of compounds based on the assumption that mass differences of atomic isotopes for different atoms can be considered to be identical [34]. Because of the extent of high resolution in FT-ICR/MS, we cannot neglect the isotope differences, i.e., it could be possible to separately detect each isotope ion containing ^2H , ^{13}C , ^{15}N and so on. But intensities of isotope compounds with isotope atoms other than ^{13}C would be too small to consider, because the

probability of ions containing ^2H , ^{15}N , and so on is much lower compared with ions containing ^{13}C . So assuming that an isotope ion $M+1$ is derived from only ^{13}C , a relative ratio of M (^{12}C) and $M+1$ (^{13}C) separated by the difference (1.0033 u) of m/z values for two peaks can allow us to estimate how many carbon atoms a compound should contain without prior information about the structure. In addition to this, MS/MS fragmentation patterns provide structural information of metabolites, so we performed MS/MS analysis for the five peaks corresponding to $m/z=(\text{A})$ 662.1037, (B) 719.4868, (C) 733.5056, (D) 747.5183, and (E) 761.5293.

In ion A, the intensity of $m/z=662.1037$ is highly correlated with those of m/z value 663.1080 in cluster 6, so those would be isotope ions, i.e., $m/z=662.1037$ (M) and $m/z=663.1080$ (M+1) because of the difference 1.0043. The number of carbon atoms estimated by the intensity ratio of 662.1037 to 663.1080 was in the range of 19 and 21 at the 99% confidence interval of the t test (Table 1). We got 845 possible molecular formulas consisting of six types of atoms (C, H, O, N, P, and S) in the range of ± 0.01 for an ion with $m/z=662.1037$. After reducing candidates that do not have the estimated number of carbon atoms, we could get 92 possible candidates, i.e., about 89% candidate molecular formulas could be considered to be not true. The candidate metabolite for ion A according to the KnapSack search (no hits in KEGG database) is nicotinamide adenine dinucleotide (NAD) ($\text{C}_{21}\text{H}_{27}\text{N}_7\text{O}_{14}\text{P}_2$), and ions obtained from MS/MS analysis ($m/z=540.0782$, 328.0532) for ion (A) are consistent with the fragmentation pattern of NAD (Fig. 3a), i.e., fragmentation ions with $m/z=540.0782$ and 328.0532 could be assigned to ($[\text{C}_{15}\text{H}_{20}\text{N}_5\text{O}_{13}\text{P}_2]^-$) [theoretical $m/z=540.0533$] and ($[\text{C}_{10}\text{H}_{11}\text{N}_5\text{O}_6\text{P}]^-$) [theoretical $m/z=328.0447$], respectively. Thus, we annotated the ions corresponding to $m/z=662.1037$ and 663.1080 in cluster 6 as NAD and also $m/z=331.0586$ in cluster 6 as a doubly charged ion ($[\text{M}-2\text{H}]^{2-}$) of NAD.

Next, we annotated four selected monoisotope ions $m/z=(\text{B})$ 719.4868, (C) 733.5056 (D) 747.5183, and (E) 761.5293. Though the candidate metabolites could not be

obtained by the database search, fragmentation ions for those were obtained by MS/MS analyses in Fig. 3b–e. In the MS/MS spectrum corresponding to the ion with $m/z=(\text{B})$ 719.4868 (Fig. 3b), two peaks for fragment ions (e.g., $m/z=253.2181$ and 255.2337) could be assigned to an unsaturated fatty acid ($\text{C}_{16}\text{H}_{30}\text{O}_2$) [theoretical $m/z=253.2167$ ($[\text{R}_2\text{O}]^-$)] and a saturated fatty acid ($\text{C}_{16}\text{H}_{32}\text{O}_2$) [theoretical $m/z=255.2324$ ($[\text{R}_1\text{O}]^-$)], indicating that the ion with $m/z=719.4868$ is a phosphatidylglycerol (PG). All ions (B–E) possess some common identifiable peaks (e.g., $m/z=255.2337$, 391.2260, 465.2628, and 483.2735 in Fig. 3b), suggesting that they are similar types of molecules, i.e., four ions, B–E, referred to as PG1 to PG4, respectively, would be different types of PGs summarized in Fig. 4a. The numbers of carbon atoms estimated at the 99% confidence interval of the t test were also true for all four ions, suggesting that identification of isotope ions based on the graph clustering and estimating the number of carbon atoms by the confidence interval of the t test could also be reliable to reduce the number of candidate molecular formulas. We also checked the effect of other constraints for reducing candidates, i.e., using element ratio constraints (H/C 0.2–3.1, O/C 0–1.2, N/C 0–1.3, P/C 0–0.3, and S/C 0–0.8) [25], but there was no impact after reducing by the t test (element ratio column in Table 1), suggesting that if we get the isotope pattern data for a metabolite in a time series, the relative ratio of isotope ions (M and M+1) can efficiently narrow down candidate molecular formulas even without other constraints. Though incorporating chromatographic separation systems into the FT-ICR/MS system is helpful to estimate the relative ratio of isotope ions and also to predict the candidate molecular formula of unknown ions in a single measurement, time series data set can also ensure the possibility of candidate molecular formulas from a statistical perspective, i.e., the confidence interval of the t test.

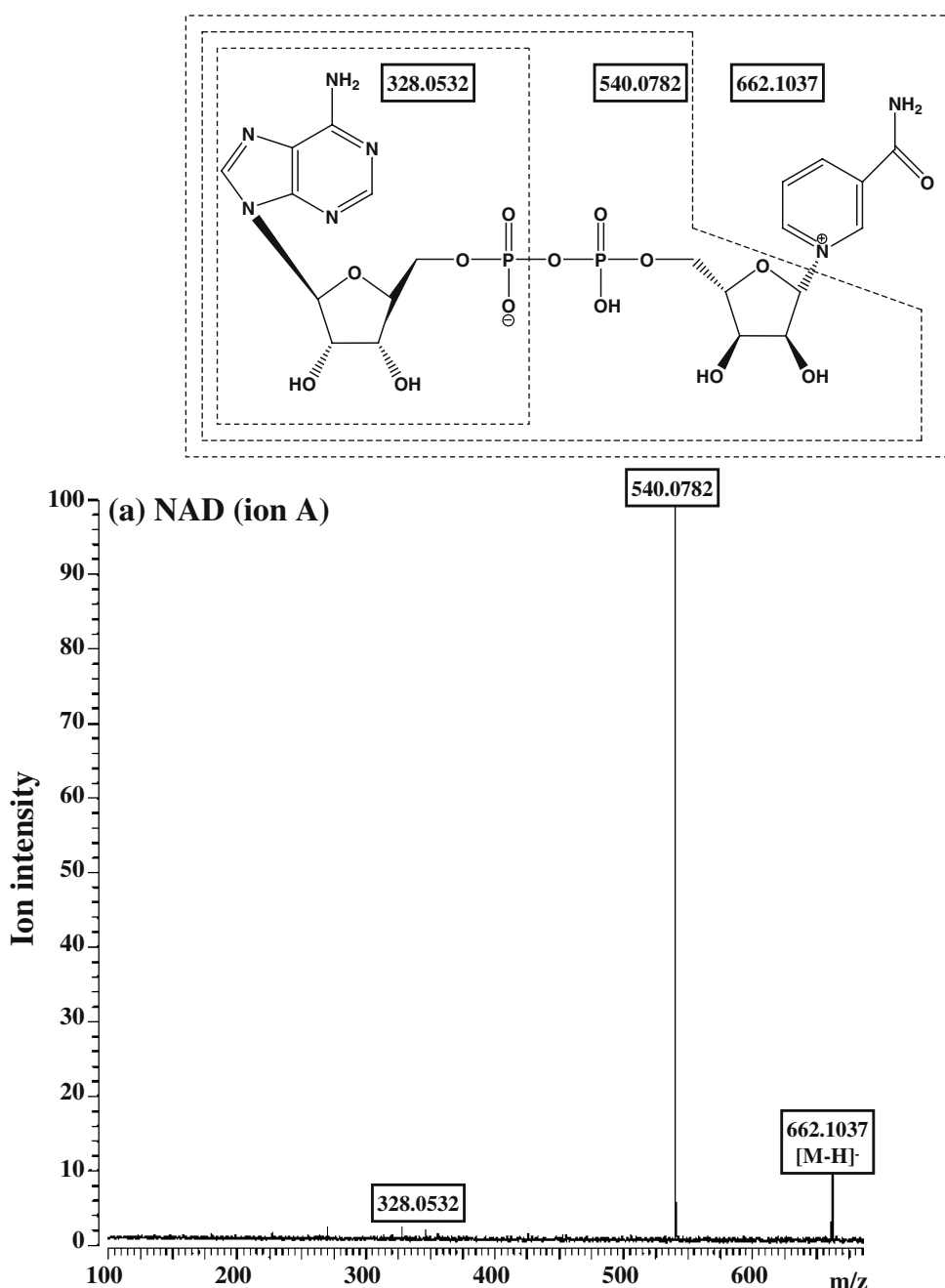
It has been reported that PGs are composed of various molecular species [35]. In the present study, another six metabolite derivative groups can be annotated as PGs by following three ‘rules’ in fatty acid metabolism (Fig. 4b):

Table 1 Summary of reduction of candidates using the isotope pattern in ions in MS/MS analyses

Ion ID	Cluster ID	Monoisotope (M)	Isotope (M+1)	Difference	Number of candidates ± 0.01	Estimated carbon number	Number of estimated candidates	Element ratio	Candidate	Actual number of carbon atoms
A	6	662.1037	663.1080	1.0044	845	19–21	92	90	NAD	21
B	1	719.4868	720.4917	1.0048	146	36–40	33	33	PG1	38
C	2	733.5056	734.5087	1.0032	167	38–44	34	34	PG2	39
D	1	747.5183	748.5227	1.0044	175	39–40	12	12	PG3	40
E	2	761.5293	762.5340	1.0047	219	28–60	102	102	PG4	41

M ‘monoisotope’ column corresponds to $[\text{M}-\text{H}]^-$ in the negative ion mode analysis

Fig. 3 MS/MS analyses of the five ions in the negative ion mode analysis. $[M-H]^-$ corresponds to the detected ion. **a** Fragmentation pattern and chemical structure of nicotinamide adenine dinucleotide (NAD) ion with $m/z=662.1037$. **b–e** Fragmentation patterns of phosphatidylglycerols 1–4 (PG1–PG4) ions with $m/z=719.4868$, $m/z=733.5056$, $m/z=747.5183$, and $m/z=761.5293$. R_1 and R_2 correspond to fatty acids



(1) Cyclopropane fatty acid (CFA) formation occurs as one of the modifications of phospholipids [36, 37]. A mass difference of 14.0157 corresponding to CFA was obtained in five pairs of PGs (PG1 and PG2, PG3 and PG4, PG5 ($m/z=691.4588$) and PG6 ($m/z=705.4757$), and PG7 ($m/z=745.5045$) and PG8 ($m/z=759.5242$), and PG9 ($m/z=773.5375$) and PG10 ($m/z=787.5556$)). (2) An elongation process occurs in fatty acids [38], i.e., a mass difference of 28.0313 u corresponds to one cycle of two-carbon addition in fatty acid biosynthesis, which was obtained in six pairs of PGs (PG5 and PG1, PG1 and PG3, PG7 and PG9, PG6 and PG2, PG2 and PG4, and PG8 and PG10). (3) A

desaturation process, i.e., a mass difference of 2.0157 was obtained in two pairs of PGs (PG3 and PG7, and PG4 and PG8). So, annotation of PG5 to PG10 could be validated by enzyme reactions in lipid metabolism.

We searched the other 174 ions using KNApSAcK, and obtained 163 metabolite candidates from the search of the entire metabolite inventory in the database. Based on the species–metabolite relationship and MS/MS analyses above, we were finally able to assign 33% of 220 detected ions to candidate metabolites. If we restrict the search to only bacteria–metabolite relations of the KNApSAcK database, then we find 26 ions are related to 38 metabolites

Fig. 3 (continued)

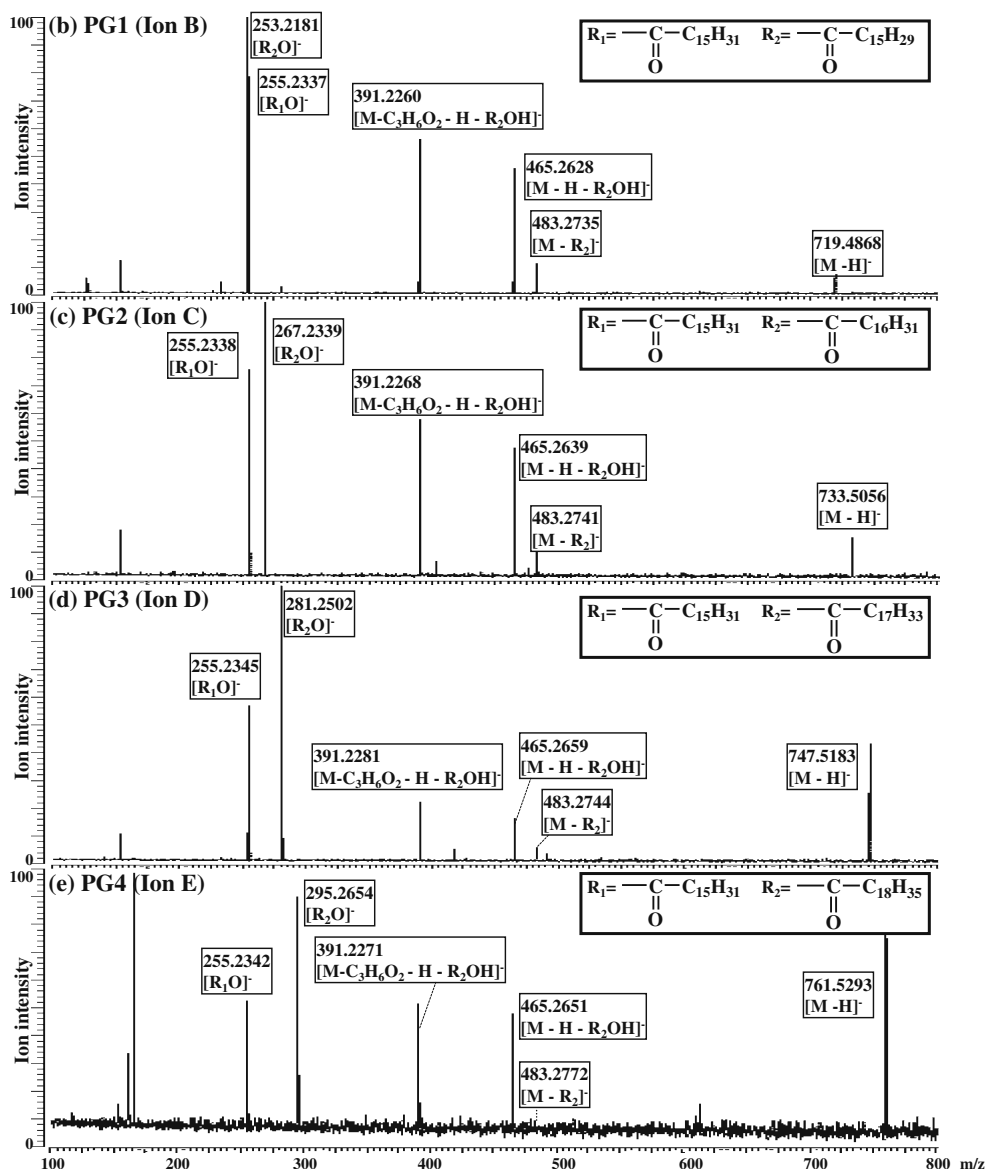


(Table 2). Out of these, there is only one whose candidates have different molecular formulas. The other 25 ions correspond to unique elemental compositions, suggesting that the information of species–metabolite relationship is efficient to extract useful lists of candidate metabolites. In this study, the percentage of ions annotated to metabolite candidates is much higher than that in the case of a plant reported by Nakamura et al. (10% of peaks in *Arabidopsis thaliana*) [9].

Cellular conditions assessed according to metabolite composition

Figure 5 shows (a) the growth curve, (b) the number of ions detected in each time point, and (c) expression profiles of metabolites in clusters 1–5. The number of ions detected in each cluster decreases toward T6 and after that increases

toward T8, suggesting that after the exponential phase, composition of metabolites in *E. coli* would be largely changed at T6.

Ions in clusters 5 and 3 correspond to ion accumulation in T2 and T3 at the exponential phase (Fig. 5c), respectively, suggesting that these metabolites would be necessary only at certain cell states. A candidate for the ion with $m/z=281.2444$ in cluster 5 obtained by KNApSack searching is oleic acid (M-12 in Fig. 2; error of $m/z=0.0042$) which is a precursor of phospholipids and has one double bond, suggesting that biosynthesis of fatty acid with double bond might occur in the exponential but not stationary phase, and other ions in cluster 5 would be compounds in a pathway related to fatty acid biosynthesis.

Candidates for the ion with $m/z=565.0503$ (M-6) in cluster 3 are UDP-D-glucose and UDP-D-galactose. Candidates for the ion with $m/z=606.0775$ (M-7) are UDP-N-

(a) Elucidated structures (PG1 to PG4)

ID	Combination of three substructures (X ₁ , X ₂ , X ₃)			
PG1	$\begin{array}{c} \text{---C---C}_{15}\text{H}_{29} \\ \\ \text{O} \end{array}$	$\begin{array}{c} \text{---C---C}_{15}\text{H}_{31} \\ \\ \text{O} \end{array}$	$\begin{array}{c} \text{OH} \\ \\ \text{---P---O---CH}_2\text{---CHOH---CH}_2\text{OH} \\ \\ \text{O} \end{array}$	$\begin{array}{ c} \text{CH}_2\text{---O---X}_1 \\ \\ \text{CH---O---X}_2 \\ \\ \text{CH}_2\text{---O---X}_3 \end{array}$
PG2	$\begin{array}{c} \text{---C---C}_{16}\text{H}_{31} \\ \\ \text{O} \end{array}$			
PG3	$\begin{array}{c} \text{---C---C}_{17}\text{H}_{33} \\ \\ \text{O} \end{array}$			
PG4	$\begin{array}{c} \text{---C---C}_{18}\text{H}_{35} \\ \\ \text{O} \end{array}$			

(b) Relation of mass differences among PG1 to 10

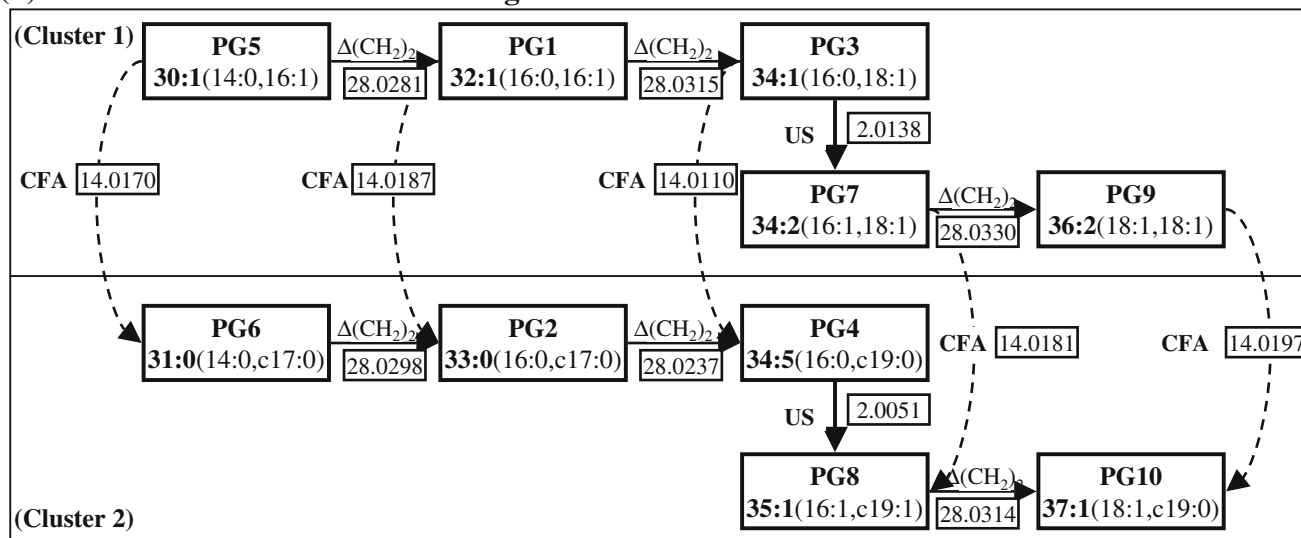


Fig. 4 Summary of phosphatidylglycerols detected in this study. **a** Molecular structures of PG1–PG4 determined by MS/MS analyses. Chemical structures in *left*, *middle*, and *right* columns correspond to substructure X₁, X₂, and X₃ of phosphatidylglycerols, respectively. **b** Relation of mass differences among PG1 to PG10. PG *xx*:*y* head-

groups, *xx* total number of carbons in the fatty acid chains, *y* number of double bonds, *c* cyclopropane, *CFA* cyclopropane fatty acid formation, *US* unsaturation. Theoretical $\Delta(\text{CH}_2)_2$, *CFA*, and *US* are 28.0313, 14.0157, and 2.0157, respectively

acetyl-D-mannosamine and UDP-N-acetyl-D-glucosamine, which are precursors of lipopolysaccharides (LPS) [39], suggesting that LPS biosynthesis would occur only in the exponential phase and relate to abundances of UDP-D-glucose and UDP-D-galactose, and other ions in cluster 3 would be compounds related to LPS biosynthesis. A candidate for the ion with $m/z=143.1080$ in cluster 3 is octanoic acid (M-4), which is the direct precursor of a vitamin, lipoic acid, and is also an exponential phase-specific metabolite. *E. coli* contains a pool of octanoic acid which can act as a substrate for lipoate ligase during lipoate starvation of a lipoic acid auxotroph [40]. The accumulation of octanoic acid at stage T3 would be needed in the

exponential phase to prepare biosynthesis of vitamins. Ions in cluster 4 correspond to ion accumulation in T7 at the stationary phase (Fig. 5c), suggesting that ions in cluster 4 would be compounds related to the stationary phase.

According to profiles in Fig. 5c, clusters 1 and 2 are exponential and stationary phase specific, respectively. It is well known that phospholipid production decreases dramatically at the stringent response [41, 42], and the bulk of CFA synthesis occurs as cultures enter the stationary phase of growth [38]. Those facts are consistent with the structures of PG2, PG4, PG6, PG8, and PG10 in cluster 2 being CFA forms of PG1, PG3, PG5, PG7, and PG9 in cluster 1, respectively. In addition to this, CFA synthesis

Table 2 Summary of candidates for ions based on KnapSack search using bacteria–metabolite relationship

Detected m/z^a	Theoretical m/z	Molecular formula	Exact mass	Error	Candidate	Species
72.9878	73.9951	C ₂ H ₂ O ₃	74.0004	0.0053	Glyoxylic acid	<i>Escherichia coli</i>
143.1080	144.1153	C ₈ H ₁₆ O ₂	144.1150	0.0003	Octanoic acid	<i>Escherichia coli</i>
253.2137	254.2210	C ₁₆ H ₃₀ O ₂	254.2246	0.0036	omega-Cycloheptanenanoic acid	<i>Alicyclobacillus acidocaldarius</i>
253.2185	254.2258	C ₁₆ H ₃₀ O ₂	254.2246	0.0012	omega-Cycloheptanenanoic acid	<i>Alicyclobacillus acidocaldarius</i>
281.2444	282.2516	C ₁₈ H ₃₄ O ₂	282.2559	0.0042	Oleic acid	<i>Escherichia coli</i>
		C ₁₈ H ₃₄ O ₂	282.2559	0.0042	<i>cis</i> -11-Octadecanoic acid	<i>Lactobacillus plantarum</i>
		C ₁₈ H ₃₄ O ₂	282.2559	0.0042	omega-Cycloheptylundecanoic acid	<i>Alicyclobacillus acidocaldarius</i>
297.2410	298.2482	C ₁₈ H ₃₄ O ₃	298.2508	0.0026	alpha-Cycloheptaneundecanoic acid	<i>Alicyclobacillus acidocaldarius</i>
297.2467	298.2540	C ₁₈ H ₃₄ O ₃	298.2508	0.0032	alpha-Cycloheptaneundecanoic acid	<i>Alicyclobacillus acidocaldarius</i>
297.2516	298.2589	C ₁₈ H ₃₄ O ₃	298.2508	0.0081	alpha-Cycloheptaneundecanoic acid	<i>Alicyclobacillus acidocaldarius</i>
321.0506	322.0579	C ₁₀ H ₁₅ N ₂ O ₈ P	322.0566	0.0013	dTMP	<i>Escherichia coli</i> K12
346.0570	347.0643	C ₁₀ H ₁₄ N ₅ O ₇ P	347.0631	0.0012	AMP	<i>Escherichia coli</i>
		C ₁₀ H ₁₄ N ₅ O ₇ P	347.0631	0.0012	3'-AMP	<i>Escherichia coli</i>
		C ₁₀ H ₁₄ N ₅ O ₇ P	347.0631	0.0012	dGMP	<i>Escherichia coli</i>
401.0168	402.0241	C ₁₀ H ₁₆ N ₂ O ₁₁ P ₂	402.0229	0.0012	dTDP	<i>Escherichia coli</i>
402.9962	404.0035	C ₉ H ₁₄ N ₂ O ₁₂ P ₂	404.0022	0.0013	UDP	<i>Escherichia coli</i>
426.0237	427.0310	C ₁₀ H ₁₅ N ₅ O ₁₀ P ₂	427.0294	0.0016	Adenosine 3',5'-bisphosphate	<i>Escherichia coli</i>
		C ₁₀ H ₁₅ N ₅ O ₁₀ P ₂	427.0294	0.0016	ADP	<i>Escherichia coli</i>
		C ₁₀ H ₁₅ N ₅ O ₁₀ P ₂	427.0294	0.0016	dGDP	<i>Escherichia coli</i>
454.0391	455.0464	C ₂₀ H ₁₉ Cl ₂ NO ₇	455.0539	0.0075	Antibiotic MI 178–34F18A2	<i>Actinomadura spiralis</i> MI178–34F18
		C ₂₀ H ₁₉ Cl ₂ NO ₇	455.0539	0.0075	Antibiotic MI 178–34F18C2	<i>Actinomadura spiralis</i> MI178–34F18
458.1112	459.1185	C ₁₅ H ₂₂ N ₇ O ₈ P	459.1267	0.0083	Phosmidosine B	<i>Streptomyces</i> sp. strain RK-16
495.1039	496.1112	C ₂₄ H ₂₀ N ₂ O ₁₀	496.1118	0.0006	Kinamycin A	<i>Streptomyces murayamaensis</i> sp. nov.
		C ₂₄ H ₂₀ N ₂ O ₁₀	496.1118	0.0006	Kinamycin C	<i>Streptomyces murayamaensis</i> sp. nov.
505.9908	506.9981	C ₁₀ H ₁₆ N ₅ O ₁₃ P ₃	506.9957	0.0023	ATP, dGTP	<i>Escherichia coli</i>
547.0756	548.0829	C ₁₆ H ₂₆ N ₂ O ₁₅ P ₂	548.0808	0.0020	dTDP-L-rhamnose	<i>Escherichia coli</i>
565.0503	566.0576	C ₁₅ H ₂₄ N ₂ O ₁₇ P ₂	566.0550	0.0025	UDP-D-glucose	<i>Escherichia coli</i>
		C ₁₅ H ₂₄ N ₂ O ₁₇ P ₂	566.0550	0.0025	UDP-D-galactose	<i>Escherichia coli</i>
606.0775	607.0848	C ₁₇ H ₂₇ N ₃ O ₁₇ P ₂	607.0816	0.0032	UDP-N-acetyl-D-mannosamine	<i>Escherichia coli</i>
		C ₁₇ H ₂₇ N ₃ O ₁₇ P ₂	607.0816	0.0032	UDP-N-acetyl-D-glucosamine	<i>Escherichia coli</i>
618.0897	619.0970	C ₁₇ H ₂₇ N ₅ O ₁₆ P ₂	619.0928	0.0042	ADP-L-glycero-beta-D-manno-heptopyranose	<i>Escherichia coli</i>
662.1037	663.1109	C ₂₁ H ₂₇ N ₇ O ₁₄ P ₂	663.1091	0.0018	NAD	<i>Escherichia coli</i>
664.1095	665.1168	C ₂₁ H ₂₉ N ₇ O ₁₄ P ₂	665.1248	0.0080	NADH	<i>Escherichia coli</i>
741.4729	742.4801	C ₃₂ H ₆₂ N ₁₂ O ₈	742.4814	0.0012	Argimicin A	<i>Sphingomonas</i> sp.
786.4712	787.4785	C ₄₁ H ₆₅ N ₅ O ₁₀	787.4731	0.0054	BE 32030B	<i>Nocardia</i> sp. A32030
853.3166	854.3239	C ₄₁ H ₄₆ N ₁₀ O ₉ S	854.3170	0.0069	Argyirin G	<i>Archangium gephyra</i> Ar 8082
		C ₄₅ H ₅₆ C ₁₂ N ₂ O ₁₀	854.3312	0.0073	Decatromicin B	<i>Actinomadura</i> sp. MK73–NF4
		C ₃₉ H ₅₀ N ₈ O ₁₂ S	854.3269	0.0030	Napsamycin C	<i>Streptomyces</i> sp. HIL Y–82,11372

^a Values correspond to the [M–H][–] ion in the negative ion mode analysis

occurs in a broad range of phosphatidylglycerols after T5. Thus, cellular conditions of *E. coli* could be explained in terms of the composition of metabolites.

Unsupervised learning such as PCA and BL-SOM makes it possible to examine metabolic phenotyping of seedlings treated with different herbicidal chemical classes

for pathway-specific inhibitions [8] and accurate classification of genes based on time series expression profiles which led to the prediction of gene functions [5, 6, 43]. Figure 6a shows the PCA projection of measurement points in time series data. The proportions, that is, percent variances to total variance, are 94.3% and 2.4% for the first and second

principal components (PC1 and PC2), respectively. So the first two principal components, which can explain 96.7% of total variance, are enough to examine the differences in eight time points. The distribution of eight time points in the first two PCs as shown in Fig. 6a implies that time points are clearly classified into two groups, an early group consisting of T1, T2, T3, T4, and T5, and a late group consisting of T6, T7, and T8, suggesting that the different growth stages could be represented by the metabolomics data. The former and latter roughly correspond to exponential and stationary phases in the growth curve of *E. coli*. This result shows that the metabolite profile in *E. coli* seems to be totally shifted from T5 to T6, which is also consistent with the transient point in the number of detected ions in Fig. 5b.

To directly relate composition of metabolites to cellular conditions, we applied partial least squares (PLS) regression to the metabolite profiling data. PLS regression provides a quantitative model to estimate the cellular conditions based on the composition of metabolites. So in the present study, we focused on the PLS model to estimate cellular conditions from exponential to stationary phase based on intensities of m/z values in FT-ICR/MS and examined quantitative differences of metabolites based on the PLS model. Growth of bacteria can be generally monitored by measuring the optical density at 600 nm (OD_{600}). A linear model for estimating the OD_{600} values according to the metabolite quantities in individual time points provides the useful information associated with quantitative differences of the metabolite between exponential and stationary phases. To attain this, we conducted PLS regression, which is applicable when the number of independent variables is very large compared with the number of samples. Using Eq. (4) the OD_{600} value can be directly estimated from the corresponding intensity vector of m/z values. When the ion has a positive value of a regression coefficient by PLS regression, its ion's level should increase from exponential to stationary phase because the optical density is saturated in the highest level of the growth curve. We got the best linear model in PLS regression with one component ($R_{pred}=0.94$). The Pearson's correlation between the observed and predicted OD_{600} values is $r=0.97$, suggesting that our constructed model would work well, and is informative to clarify the relation between a growth stage and metabolite profile. Next, we plotted the regression coefficients of each ion determined by using the proposed model in order to elucidate which metabolite is important for estimating the OD_{600} values (Fig. 6b). The ions with negative and positive coefficients contribute to the constructed model, negatively and positively, and are dominant in exponential and stationary phase, respectively. Four ions (PG1, $m/z=719.4868$; PG2, $m/z=733.5056$; PG3, $m/z=747.5183$; PG4, $m/z=761.5293$) which were analyzed by MS/MS analysis as described

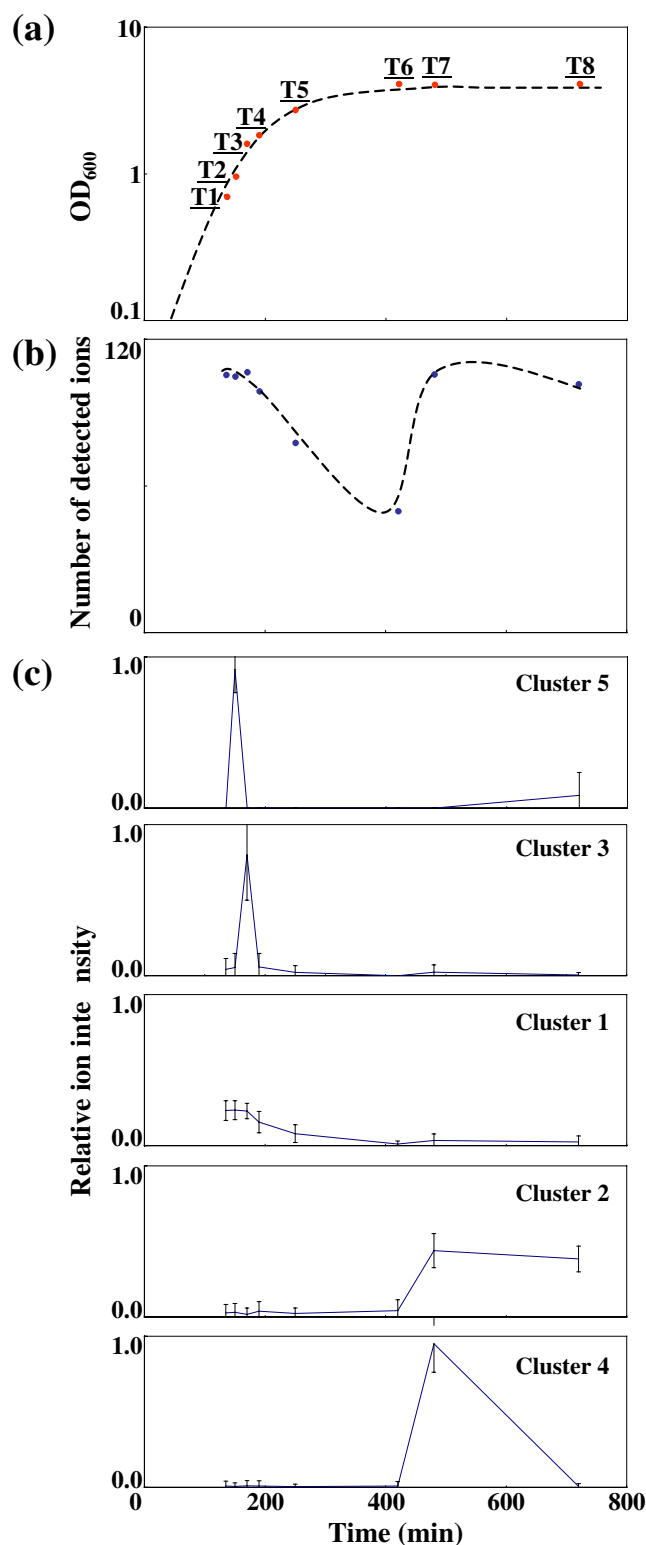


Fig. 5 a Growth curve. b Time series change of total number of detected ions in each time point. c Average expression profiles of ions in clusters 1–5. Error bars show standard deviation in each time point

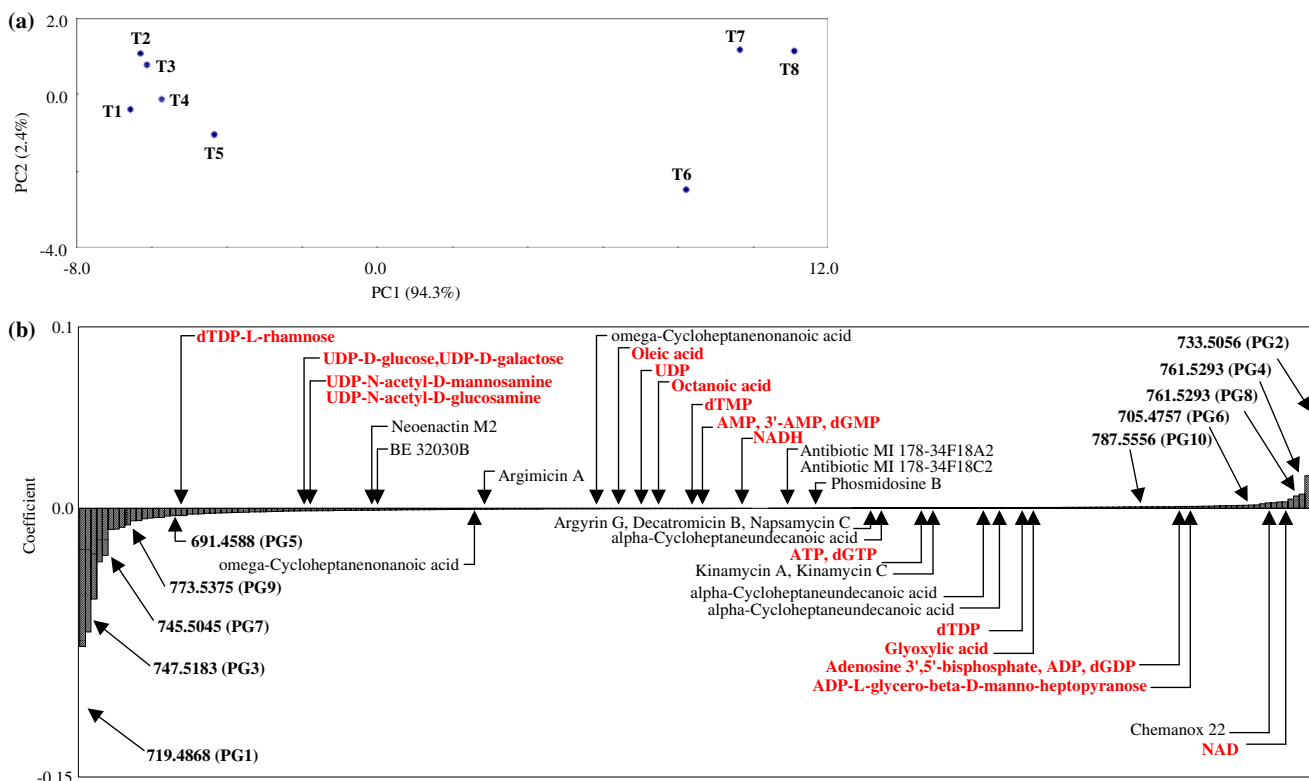


Fig. 6 PCA and PLS analyses. **a** Plot of eight time points using the first two PCs and **b** intensity of regression coefficients when the PLS model equation is transformed into a linear regression-like formula.

The metabolites written in *red* are reported metabolites in *E. coli*. The metabolites written in *black* are reported metabolites in other bacteria species

above had the highest coefficients. Other annotated six ions (PG5, $m/z=691.4588$; PG6, $m/z=705.4757$; PG7, $m/z=745.5045$; PG8, $m/z=759.5242$; PG9, $m/z=773.5375$; PG10, $m/z=787.5556$) also had higher coefficients, suggesting that PLS analysis could extract stage-specific metabolites efficiently. Thus, the observed behavior of metabolites is highly reflected in the regression coefficients of the PLS model and the interpretation of the coefficients is fairly consistent with the transition of metabolites from exponential to stationary phase.

Conclusions

This study presents a metabolomics approach to analyze growth-specific metabolites of bacteria, based on the FT-ICR/MS platform. Correlation analyses can make it possible to predict unknown molecular structure using isotope ratios by way of grouping metabolite derivative ions. Though 1-ppm mass accuracy alone is insufficient for unique elemental composition assignment [33], integrated analysis based on information of isotope relation, fragmentation patterns by MS/MS analysis, and co-occurring metabolites can make it possible to annotate ions as metabolites and estimate cellular conditions based on metabolite compo-

sition. PCA revealed the differences between the growth stages on the basis of 220 independent metabolites, suggesting that metabolic profiling is a useful method for distinguishing the growth stages. Using PLS regression we constructed a linear relationship between OD_{600} values and metabolite profiles. High correlation between predicted and observed OD_{600} values certifies the correctness of the linear model. Our analyses reveal that global CFA formation of PGs occurs as *E. coli* enters the stationary phase from the exponential phase. The results indicate that nontargeted metabolomics based on direct-infusion FT-ICR/MS is useful for analyzing the responses of biological systems to a variety of changes. Our integrated methodology is applicable to metabolic studies involving other organisms.

Acknowledgements This work was supported by a Grant-in-Aid for Scientific Research on Priority Areas, "Systems genomics", from the Ministry of Education, Culture, Sports, Science and Technology of Japan and the BIRD project "Metabolome-Mass Spectral Database" from Japan Science and Technology Agency.

Open Access This article is distributed under the terms of the Creative Commons Attribution Noncommercial License which permits any noncommercial use, distribution, and reproduction in any medium, provided the original author(s) and source are credited.

References

1. Fiehn O (2002) *Plant Mol Biol* 48:155–171
2. Villas-Boas SG, Rasmussen S, Lane GA (2005) *Trends Biotechnol* 23:385–386
3. Marshall AG, Hendrickson CL, Shi SD (2002) *Anal Chem* 74:252A–259A
4. Aharoni A, Ric de Vos CH, Verhoeven HA, Maliepaard CA, Kruppa G, Bino R, Goodenowe DB (2002) *Omics* 6:217–234
5. Hirai MY, Klein M, Fujikawa Y, Yano M, Goodenowe DB, Yamazaki Y, Kanaya S, Nakamura Y, Kitayama M, Suzuki H, Sakurai N, Shibata D, Tokuhisa J, Reichelt M, Gershenzon J, Papenbrock J, Saito K (2005) *J Biol Chem* 280:25590–25595
6. Hirai MY, Yano M, Goodenowe DB, Kanaya S, Kimura T, Awazuhara M, Arita M, Fujiwara T, Saito K (2004) *Proc Natl Acad Sci USA* 101:10205–10210
7. Tohge T, Nishiyama Y, Hirai MY, Yano M, Nakajima J, Awazuhara M, Inoue E, Takahashi H, Goodenowe DB, Kitayama M, Noji M, Yamazaki M, Saito K (2005) *Plant J* 42:218–235
8. Oikawa A, Nakamura Y, Ogura T, Kimura A, Suzuki H, Sakurai N, Shinbo Y, Shibata D, Kanaya S, Ohta D (2006) *Plant Physiol* 142:398–413
9. Nakamura Y, Kimura A, Saga H, Oikawa A, Shinbo Y, Kai K, Sakurai N, Suzuki H, Kitayama M, Shibata D, Kanaya S, Ohta D (2007) *Planta* 227:57–66
10. Suzuki H, Sasaki R, Ogata Y, Nakamura Y, Sakurai N, Kitajima M, Takayama H, Kanaya S, Aoki K, Shibata D, Saito K (2008) *Phytochemistry* 69:99–111
11. Hall RD (2006) *New Phytol* 169:453–468
12. Stein L (2001) *Nat Rev Genet* 2:493–503
13. Soga T, Ohashi Y, Ueno Y, Naraoka H, Tomita M, Nishioka T (2003) *J Proteome Res* 2:488–494
14. Gauthier JW, Trautman TR, Jacobson DB (1991) *Anal Chim Acta* 246:211–225
15. Laskin J, Futrell JH (2005) *Mass Spectrom Rev* 24:135–167
16. Kanaya S, Kinouchi M, Abe T, Kudo Y, Yamada Y, Nishi T, Mori H, Ikemura T (2001) *Gene* 276:89–99
17. Abe T, Kanaya S, Kinouchi M, Ichiba Y, Kozuki T, Ikemura T (2003) *Genome Res* 13:693–702
18. Boulesteix AL, Strimmer K (2007) *Brief Bioinform* 8:32–44
19. Altaf-Ul-Amin M, Shinbo Y, Mihara K, Kurokawa K, Kanaya S (2006) *BMC Bioinformatics* 7:207
20. Shinbo Y, Nakamura Y, Altaf-Ul-Amin M, Asahi H, Kurokawa K, Arita M, Saito K, Ohta D, Shibata D, Kanaya S (2006) In: Saito K, Dixon RA Willmitzer L (eds) *Plant metabolomics. Biotechnology in agriculture and forestry*, vol 57. Springer, Berlin, pp 165–181
21. Brauer MJ, Yuan J, Bennett BD, Lu W, Kimball E, Botstein D, Rabinowitz JD (2006) *Proc Natl Acad Sci USA* 103:19302–19307
22. Bairoch A (2000) *Nucleic Acids Res* 28:304–305
23. Goto S, Okuno Y, Hattori M, Nishioka T, Kanehisa M (2002) *Nucleic Acids Res* 30:402–404
24. Kanehisa M, Goto S, Hattori M, Aoki-Kinoshita KF, Itoh M, Kawashima S, Katayama T, Araki M, Hirakawa M (2006) *Nucleic Acids Res* 34:D354–D357
25. Kind T, Fiehn O (2007) *BMC Bioinformatics* 8:105
26. Tautenhahn R, Boettcher C, Neumann S (2007) *Proceedings of BIRD 2007-1st international conference on bioinformatics research and development*. LNBI 4414. Springer-Verlag, Berlin. Available via <http://msbi.ipb-halle.de/~rtautenh/bird07.pdf>. Accessed 27 May 2008
27. Fisher R (1958) In: Fisher RA (ed) *Statistical methods for research workers*, 13th edn. Oliver & Boyd, Edinburgh
28. Fiehn O, Wohlgenuth G, Scholz M (2005) LNBI 3615. Springer-Verlag, Berlin, pp 224–239
29. Scholz M, Fiehn O (2007) *Pac Symp Biocomput* 169–180
30. Wheeler DL, Barrett T, Benson DA, Bryant SH, Canese K, Chetvermin V, Church DM, DiCuccio M, Edgar R, Federhen S, Geer LY, Helmberg W, Kapustin Y, Kenton DL, Khovayko O, Lipman DJ, Madden TL, Maglott DR, Ostell J, Pruitt KD, Schuler GD, Schriml LM, Sequeira E, Sherry ST, Sirotkin K, Souvorov A, Starchenko G, Suzek TO, Tatusov R, Tatusova TA, Wagner L, Yaschenko E (2006) *Nucleic Acids Res* 34:D173–D180
31. De Luca V, St Pierre B (2000) *Trends Plant Sci* 5:168–173
32. De Laeter JR, Bohlke JK, De Bièvre P, Hidaka H, Pieser HS, Rosman KJR, Taylor PDP (2003) *Pure Appl Chem* 75(6):683–800
33. Kind T, Fiehn O (2006) *BMC Bioinformatics* 7:234
34. Boecker S, Letzel MC, Lipták Z, Pervukhin A (2006) *WABI:12*
35. Ishinaga M, Kanamoto R, Kito M (1979) *J Biochem (Tokyo)* 86:161–165
36. Chang YY, Cronan JE Jr (1999) *Mol Microbiol* 33:249–259
37. Grogan DW, Cronan JE Jr (1997) *Microbiol Mol Biol Rev* 61:429–441
38. Magnuson K, Jackowski S, Rock CO, Cronan JE Jr (1993) *Microbiol Rev* 57:522–542
39. Vimr ER, Kalivoda KA, Deszo EL, Steenbergen SM (2004) *Microbiol Mol Biol Rev* 68:132–153
40. Ali ST, Moir AJ, Ashton PR, Engel PC, Guest JR (1990) *Mol Microbiol* 4:943–950
41. Merlie JP, Pizer LI (1973) *J Bacteriol* 116:355–366
42. Polakis SE, Guchhait RB, Lane MD (1973) *J Biol Chem* 248:7957–7966
43. Yano M, Kanaya S, Altaf-Ul-Amin M, Kurokawa K, Hirai MY, Saito K (2006) *J Comput Aided Chem* 7:125–136